The above discussion assumes that $F(Kr)$ for PDW can be used to apply a correction for trapped modern air and hence deduce $^{40}Ar/^{4}He$ ratios for the vent fluids. Elemental fractionation may occur during boiling, because solubility increases with atomic mass, and could render the correction invalid. At high temperatures, however, solubilities of the different noble gases converge[26], generating negligible fractionation[27]. Furthermore, vent fluids from the southern Juan de Fuca ridge have relative abundance patterns identical to those of air-saturated sea water at 2 °C, even though boiling has led to gas loss[28]. In contrast, vent fluids at 21° N have Ne concentrations comparable to those of Pacific deep water[6] and thus reveal no depletion that would result from phase separation.

Detailed interpretations of He isotope and helium/heat ratios in vent fluids at 21° N have been adequately treated elsewhere[6,8]. Here, our purpose is rather to demonstrate that measurements currently made by sampling deep ocean water can be made on trapped fluids in sulphides from the sea floor. This work could be extended to fluids in a wide range of hydrothermal deposits as a way of studying helium/heat regimes and mantle $^{3}He/^{4}He$ ratios past and present. Future work on transparent minerals will allow noble gas extractions to be combined with microthermometric measurements of trapping temperatures in individual inclusions. With opaque minerals, it will be necessary to determine precipitation temperatures from microthermometric measurements of fluids trapped by coexisting transparent minerals and associate this with the average $^{40}Ar/^{4}He$ ratio. Equation (2) does not rely explicitly on the measurement of ^{3}He and could be applied, with simultaneous laser ablation studies of H_2O and the noble gases[29], to the analysis of individual fluid inclusions, where ^{3}He is below the limits of detection. But like equation (1), this assumes a two-component mixture and would be invalidated by the presence of radiogenic ^{4}He and ^{40}Ar, and it would be necessary to establish the presence of mantle $^{3}He/^{4}He$ ratios by bulk measurements. □

Received 20 March; accepted 5 May 1992.

1. Canadian-American Seamount Expedition *Nature* **313,** 212-214 (1985).
2. Lupton, J. E., Baker, E. T. & Massoth, G. J. *Nature* **337,** 161-164 (1989).
3. O'Nions, R. K. & Oxburgh, E. R. *Nature* **306,** 429-431 (1983).
4. Sclater, J. G. *et al. J. geophys. Res.* **86,** 11535-11552 (1981).
5. Jenkins, W. J. *et al. Nature* **272,** 156-158 (1978).
6. Lupton, J. E. *et al. Earth planet. Sci. Lett.* **50,** 115-127 (1980).
7. Lupton, J. E. *Eos* **64,** 723 (1983).
8. Welhan, J. A. & Craig, H. in *Hydrothermal Processes at Seafloor Spreading Centers* (eds Rona, P. A., Bostrom, K., Laubier, L. & Smith, K. L.) (Plenum, New York, 1983).
9. Craig, H., Welhan, J. A. & Hilton, D. R. *Eos* **68,** 1553 (1987).
10. Rosenberg, N. D. *et al. Nature* **334,** 604-607 (1988).
11. Baker, E. T. & Lupton, J. E. *Nature* **346,** 556-558 (1990).
12. Simmons *et al. Nature* **329,** 429-432 (1987).
13. RISE Project group *Science* **207,** 1421-1449 (1980).
14. Allegre, C. J., Staudacher, Th. & Sarda, Ph. *Earth planet. Sci. Lett.* **81,** 127-150 (1986/87).
15. Staudacher, Th. *et al. Earth planet. Sci. Lett.* **96,** 119-133 (1989).
16. Stuart, F. M. & Turner, G. *Chem. Geol.* (in the press).
17. Clarke, W. B., Beg, M. A. & Craig, H. *Earth planet. Sci. Lett.* **6,** 212-220 (1969).
18. Bieri, R. H. & Koide, M. *J. geophys. Res.* **77,** 1667-1676 (1972).
19. Bohlke, J. K. & Irwin, J. J. *Geochim. cosmochim. Acta* **56,** 187-203 (1992).
20. Smith, S. P. & Kennedy, B. M. *Geochim. cosmochim. Acta* **47,** 503-515 (1983).
21. Kelley, D. S. & Delaney, J. R. *Earth planet. Sci. Lett.* **83,** 53-66 (1987).
22. Cowan, J. & Cann, J. *Nature* **333,** 259-261 (1988).
23. Ozima, M. & Zashu, S. *Earth planet. Sci. Lett.* **62,** 24-40 (1983).
24. Woodruff, L. & Shanks, W. C. III *J. geophys. Res.* **93,** 4562-4572 (1988).
25. Crowe *et al. Chem. Geol.* (in the press).
26. Potter, R. & Clyne, M. A. *J. Solution Chem.* **7,** 837-844 (1976).
27. Mazor, E. & Truesdell, A. H. *Geothermics* **13,** 91-102 (1984).
28. Kennedy, B. M. *Geochim. cosmochim. Acta* **52,** 1929-1935 (1988).
29. Burnard, P. *et al. Proc. 7th Conf. Water-Rock Interaction* 7 (in the press).

ACKNOWLEDGEMENTS. We thank the pilots and scientists aboard the 1979 and 1981 ALVIN expeditions and P. Duller for the provision of the samples. We thank D. J. Blagburn for technical assistance, P. Schofield for XRD analyses and J. Maynard for sulphur isotope measurements. Financial support from NERC and NSF is gratefully acknowledged.

Crustal control of ridge segmentation inferred from observations of the Reykjanes Ridge

R. E. Bell & W. R. Buck

Lamont-Doherty Geological Observatory of Columbia University, Palisades, New York 10964, USA

LARGE-AMPLITUDE variations in topography and inferred crustal thickness along the axes of mid-ocean ridges, often referred to as segmentation[1], are mainly observed at slow-spreading ridges[2–4]. This observation has led to the suggestion that mantle processes give rise to segmentation only when spreading rates are low[5,6]. Here we make the alternative proposal that the development of segmentation is controlled by the temperature of the crust: segmentation cannot develop when the lower crust is hot enough to undergo rapid ductile flow. Thermal models predict that thick crust at a slow-spreading ridge may be as hot as normal-thickness crust along fast-spreading ridges; we accordingly test our hypothesis at a slow-spreading ridge characterized by thick crust—the Reykjanes Ridge. Topography and gravity data along the Reykjanes Ridge axis indeed show an absence of segmentation, suggesting that the thermal state of the crust, rather than any mantle process, controls the development of this structure.

The structure of mid-ocean ridges has long been inferred from gravity and bathymetry data[7,8]. Recently, long sections of both fast- and slow-spreading ridges have been surveyed with multibeam bathymetry and high-resolution gravimeters[1,2,3,9,10]. The results show that along-axis variations in gravity and topography at slow ridges are generally much greater than at fast-spreading ridges. The distinctive gravity and topography signature of slow-spreading ridges can be explained by along-axis crustal thickness variations of up to three kilometres[1]. In contrast, large crustal thickness variations are not required to explain the small along-axis variations in gravity and topography documented at fast-spreading ridges[9].

Very different processes must act at slow- and fast-spreading ridges to explain the contrasting axial crustal structures inferred from topography and gravity data. Parmentier and Phipps-Morgan[5] suggest that the mode of mantle flow is dependent on spreading rate: fast-spreading ridges are dominated by sheet-like upwelling and slow-spreading ridges are dominated by diapiric upwelling (Fig. 1*a*). Sheet-like upwelling at fast ridges will supply a constant amount of melt along axis resulting in a constant crustal thickness. Diapiric upwelling along slow-spreading ridges should cause greater melting and thicker axial crust at the centres of upwelling. A second possibility is that diapiric mantle upwelling is ubiquitous, but at some ridges crustal flow evens out differences in crustal thickness. At a fast-spreading ridge, the hot crust may flow too rapidly to maintain crustal thickness variations, whereas at a slow-spreading ridge, the cold crust locks in variations in thickness resulting from diapiric mantle flow (Fig. 1*b*).

At a slow-spreading ridge with thick and presumably hot axial crust, the model based on differences in mantle flow would predict large along-axis variations in crustal thickness, whereas the model based on differences in crustal flow would predict little variation. Here we use gravity and topography data from the hot, slow-spreading Reykjanes Ridge to test for along-axis crustal thickness variations.

A mantle Bouguer anomaly is constructed from a free-air gravity anomaly by removing the gravitational effect of the crust–water interface and the effect of a constant-thickness crust[9]. The resulting anomalies reflect deviations from the assumed density structure of the crust or mantle. Along 325 km of the Mid-Atlantic Ridge, south of the Atlantis Fracture Zone,

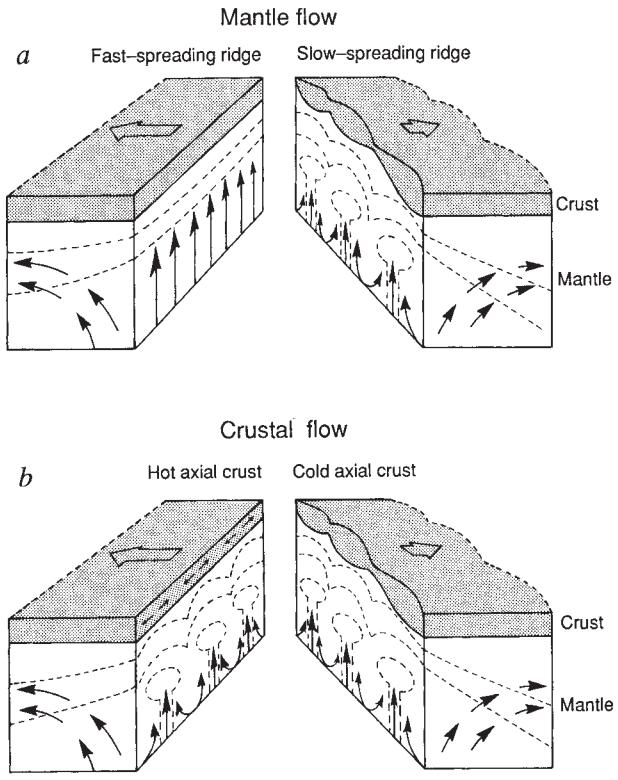

FIG. 1 Schematic illustration of two mechanisms for producing along-axis segmentation at slow-spreading ridges. *a*, Mantle flow model. In this model the segmentation is the result of diapiric mantle upwelling beneath slow-spreading ridges (right) represented by heavy arrows resulting in regions of focused upward flow causing thicker crust above upwelling centres. Beneath fast-spreading ridges (left), the upward flow of the mantle is uniform or sheet-like resulting in constant crustal thickness along the axis. The crust is simply a passive recorder of the changing patterns of mantle upwelling. The figure is modified from ref. 6. *b*, Crustal flow model. In this model the upwelling mantle is diapiric beneath all ridges. The variations in crustal thickness caused by this diapirism are only preserved when the crustal flow is sluggish (that is when the crust is cold, as for the case at the right). When the axial crust is hot, it can flow fast enough to even out any significant crustal thickness variations, as shown at the left. The arrows within the crustal section of the hot axial crust illustration indicate this flow of material away from the upwelling centres.

Lin *et al.*[1] calculated a mantle Bouguer anomaly with a full two-dimensional data set. We have used the axial bathymetry and free-air gravity data from this area to demonstrate the validity of a calculation based on a single axial profile. The segmentation recognized in the two-dimensional data is clearly visible in the single along-axis profile (Fig. 2). Some of the difference between the simple axial calculation and the two-dimensional treatment probably arises from variations in the rift flank topography. The smoothness of the axial topography along the Reykjanes Ridge should minimize the contribution of this potential error source.

The Reykjanes Ridge is the portion of the Mid-Atlantic Ridge extending over 1,200 km from Iceland south to the Charlie Gibbs Fracture Zone (Fig. 3). The Reykjanes Ridge, spreading at a half rate of 1 cm yr^{-1} (refs 7, 11), lacks the distinct axial valley characteristic of most slow-spreading ridges. The axial high along the Reykjanes Ridge resembles the topography of the fast-spreading East Pacific Rise. The crust along the ridge varies from 8 to 10 km thickness[12,13] in contrast to normal oceanic crustal thicknesses of 5–6 km (ref. 14). The Reykjanes Ridge has an average depth of 1,000 m, whereas the average depth of the Mid-Atlantic Ridge south of the Atlantis Fracture Zone is ~3,000 m (refs 1, 10). The isotope signature of basalts along the axis of the Reykjanes Ridge indicates that the thick crust and shallow water depth are associated with the Iceland hotspot[15].

Our geophysical data were collected during a RV *Vema* cruise along the Reykjanes Ridge (Fig. 3). For 83 crossings made during the entire cruise, the r.m.s. errors were 4.2 mGal with a mean of 0.9 mGal for the gravity and 58.6 m with a mean of 2.5 m for the topographic data. Analysis of the profiles evaluated here results in r.m.s. errors of 3.6 mGal and 64.3 m for seven crossovers.

Along the Reykjanes Ridge, we calculated mantle Bouguer anomalies from both a single along-ridge profile centred along the axial magnetic anomaly and the long lines perpendicular to

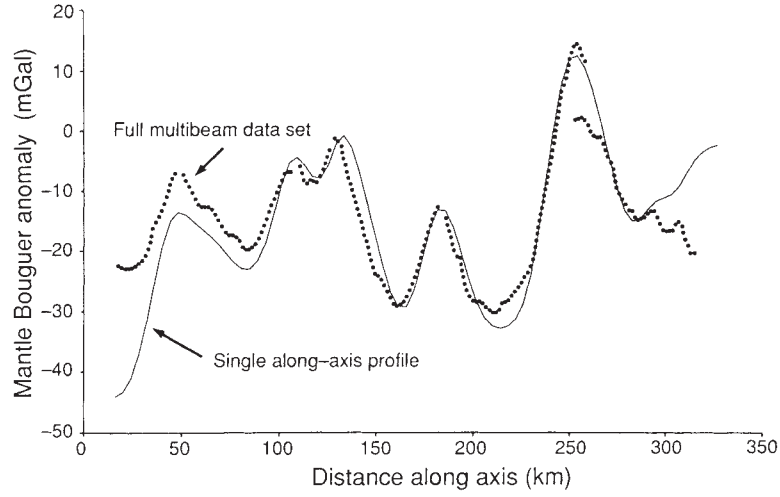

FIG. 2 Mantle Bouguer anomaly along the ridge axis south of the Atlantis Fracture Zone. The dotted line is the axial profile extracted from a full two-dimensional study[5]. The solid line is the mantle Bouguer anomaly calculated from a single along-axis profile resampled from the Lin *et al.*[1] data.

the ridge using a crustal density of 2,700 kg m^{-3} and a 9-km-thick crust. The r.m.s. difference between the axial mantle Bouguer anomaly and the ridge perpendicular calculations is 5.2 mGal for the seven crossovers (Fig. 4*a*). The striking features of the Reykjanes mantle Bouguer anomaly are the small-amplitude (5–10 mGal) short-wavelength (10–25 km) anomalies superimposed a regional gradient, and the general absence of high-amplitude (10–60 mGal) long-wavelength (35–75 km) variations observed along other slow-spreading ridges.

These short-wavelength anomalies either arise from density variations in the upper crust or are artefacts of the one-dimensional assumption inherent in the calculation. A 5% density variation in the upper crust or a 200-m topographic feature ignored in the one-dimensional calculation could produce this signal. A Moho source for these anomalies is unlikely because of the amplitude and wavelength of crustal thickness variations required. Forward modelling demonstrates that the crustal thickness variations required to explain these anomalies are double the thickness variations proposed along other slow-spreading ridges and much shorter wavelength.

The uniqueness of the mantle Bouguer anomaly along the Reykjanes Ridge is best illustrated by comparisons with other mid-ocean ridges (Fig. 4*b*). The Reykjanes Ridge lacks the large anomalies observed at slow-spreading ridges in the North and South Atlantic. We have upward continued the mantle Bouguer anomaly to a distance of 3,000 m from the sea floor to simulate an anomaly along a typical, deeper mid-ocean ridge. This upward continued Reykjanes Ridge anomaly retains a higher-frequency signal than the fast-spreading East Pacific Rise. The Reykjanes Ridge also lacks large (700–1,500 m) variations in axial depth observed along other slow-spreading ridges. Thus neither the gravity nor the topography indicates along-axis variations in the crustal thickness at the Reykjanes Ridge.

Other characteristics of this slow-spreading ridge are its anomalously thick crust and associated higher crustal temperatures. Crust formed at fast-spreading ridges is also hotter than crust along typical slow-spreading ridges. These observations imply that the temperature of the crust controls whether large-amplitude segmentation develops along a ridge. The segmentation of crustal thickness along ridges may be a consequence of mantle diapirism or may be related to lithospheric processes. Whatever mechanism causes segmentation at slow-spreading ridges, it cannot produce segmentation wherever crustal temperatures are evaluated.

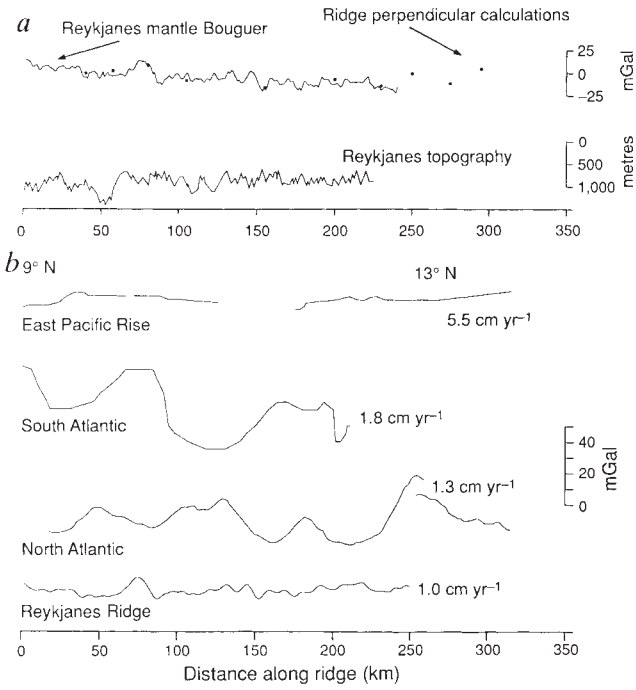

FIG. 4 *a*, Mantle Bouguer anomaly along the Reykjanes Ridge. The upper profile is the result of the axial profile calculations and the dots result from the calculations of the axis perpendicular lines. The axial topography profile is below the mantle Bouguer anomaly. *b*, Mantle Bouguer anomalies along spreading ridges with a wide variety of spreading rates. The absolute values of the profiles were offset to facilitate the comparison. The top profiles are from two locations along the East Pacific Rise[2]. The left-hand values are from 9° N and the right-hand samples are from 13° N. The second profile is the mantle Bouguer anomaly calculated by Kuo and Forsyth[9] from the South Atlantic. The mantle Bouguer anomaly calculated by Lin *et al.*[1] for the region in the North Atlantic south of the Atlantis Fracture Zone is next. The Reykjanes Ridge anomaly, with the long-wavelength trend removed, and upward continued to simulate an average axial depth of 3,000 m, is illustrated at the bottom.

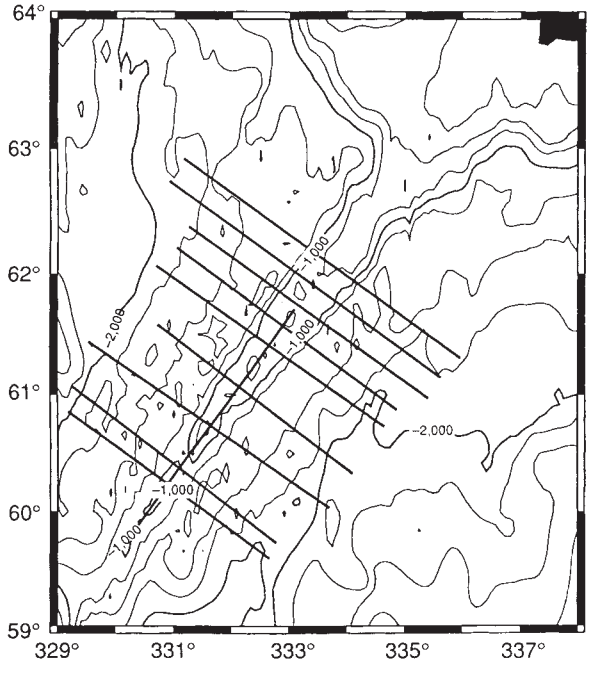

FIG. 3 Bathymetry of the Reykjanes Ridge, south of Iceland, contoured at 250-m intervals. Iceland is in the northeast corner. The tracklines from the Vema 23 cruise[7] are superimposed on the bathymetry.

The strength and viscosity of crustal rocks is a strong function of temperature. Because the crust of the Reykjanes Ridge is much thicker than typical oceanic crust, the base of the crust should be much hotter than at other slow-spreading ridges. A simple analytical model can be used to illustrate the effect of plate velocity and crustal thickness on the lower crustal temperature. In this one-dimensional model we assume a constant upward velocity equal to the plate velocity. The boundary conditions applied to the heat-flow equation are that the upper surface is at 0 °C and the temperature at infinite depth is 1,300 °C. The thermal diffusivity is taken to be 10^{-6} m^2 s^{-1}. For a plate velocity of 1 cm yr^{-1} a crustal temperature greater than 1,150 °C will only be achieved for thicknesses greater than 6.8 km. At a faster rate of 5 cm yr^{-1} this temperature is reached at 1.36 km depth. Many effects could alter these numbers, including hydrothermal circulation and advection of magma[16].

Thick crust at slow-spreading ridges or normal crust at fast-spreading ridges may be hot enough partially to melt, and a steady-state magma chamber may be present. Even if a steady-state magma chamber is absent, the lower crust may be weak enough to flow rapidly. To estimate the conditions needed for flow to remove topographic variations, we approximate the flow of a crustal layer as a channel flow[17,18]. Because crust cools as it moves away from a spreading centre, there is limited time for

crustal flow to operate. A continuous magma chamber as thin as 3 cm filled with basaltic melt having a viscosity of 10 Pa s could remove 50-km-wavelength topographic variations within 10,000 years. Alternatively, if 3 km of lower crust had a viscosity of 10^{16} Pa s then topography would decay at the same rate.

It has been suggested that crustal rheology determines the presence or absence of axial valleys[19,20]. Axial valleys are prominent along most slow-spreading ridges, but are absent along most fast-spreading ridges. The presence of either a long-lived magma chamber or very weak crust is thought to preclude the formation of a prominent axial valley. Our results suggest that crustal flow is as important in crustal segmentation as it is in determining the form of across-ridge topography. □

Received 3 March; accepted 23 April 1992.

1. Lin, J., Purdy, G. M., Schouten, H., Sempere, J. C. & Zervas, C. *Nature* **344,** 627–632 (1990).
2. Madsen, J. A., Detrick, R. S., Mutter, J. C., Buhl, R. & Orcutt, J. A. *J. geophys. Res.* **95,** 4967–4987 (1990).
3. Morris, E. & Detrick, R. S. *J. geophys. Res.* **96,** 4355–4366 (1991).
4. Blackman, D. K. & Forsyth, D. W. *J. geophys. Rev.* **96,** 11741–11758 (1991).
5. Parmentier, E. M. & Phipps-Morgan, J. *Nature* **348,** 325–328 (1990).
6. Lin, J. & Phipps-Morgan, J. *Geophys. Res. Lett.* **19,** 13–16 (1992).
7. Talwani, M., Windisch, C. C. & Langseth, M. G. *J. geophys. Res.* **76,** 473–517 (1971).
8. Woodside, J. M. *Can. J. Earth Sci.* **9,** 942–959 (1972).
9. Kuo, B. & Forsyth, D. W. *Mar. geophys. Res.* **10,** 205–232 (1988).
10. Sempéré, J.-C., Purdy, G. M. & Schouten, H. *Nature* **344,** 427–431 (1990).
11. Vogt, Peter R. in *The Geology of North America*, Vol. M (eds Vogt, P. & Tucholke, B.) 189–204 (Geological Society of America, Boulder, 1986).
12. Bunch, A. & Kennett, B. L. N. *Geophys. J. R. astr. Soc.* **61,** 141–166 (1980).
13. RRISP *J. Geophys.* **47,** 228–238 (1980).
14. Purdy, G. M. and Ewing, J. in *The Geology of North America*, Vol. M (eds Vogt, P. & Tucholke, B.) 313–330 (Geological Society of America, Boulder, 1986).
15. Schilling, J. G. *The Geology of North America*, Vol. M (eds Vogt, P. & Tucholke, B). 137–156 (Geological Society of America, Boulder, 1986).
16. Chen, Y. & Morgan, W. J. *J. geophys. Res.* **95,** 9275–9282 (1989).
17. Turcotte, D. L. & Schubert, G. *Geodynamics: Applications of Continuum Physics to Geological Problems* (Wiley, New York, 1982).
18. Bird, P. *J. geophys. Res.* **96,** 10275–10286 (1991).
19. MacDonald, K. C., Scheirer, D. S. & Carbotte, S. M. *Science* **253,** 986–994 (1991).
20. Wilson, D. S., Clague, D. A., Sleep, N. H. & Morton, J. L. *J. geophys. Res.* **93,** 11974–11984 (1988).

ACKNOWLEDGEMENTS. We thank J. Cochran, J. Mutter, J. Lin, M. Spiegelman and P. Flemings for their comments. This work was supported by the NSF and the Office of Naval Research.

Desert ants on a thermal tightrope

R. Wehner*, A. C. Marsh† & S. Wehner*

* Department of Zoology, University of Zurich, Winterthurerstrasse 190, CH-8057 Zurich, Switzerland
† Department of Zoology, University of Namibia, PB 13301, Windhoek, Namibia

MANY animals restrict their foraging activities to certain times of the day or night, but the Saharan silver ant *Cataglyphis bombycina* is exceptional in that all foragers leave their underground nest in an explosive outburst confined to a few minutes per day during the hottest midday period. The foraging activity of this 'thermophilic' ant is compressed into a small thermal window by predatory pressure on the one hand and heat stress on the other.

On a summer day in the central Sahara, the silver ant, *C. bombycina*, is the only arthropod that forages in the full midday sun, even when surface temperatures exceed 60 °C (refs 1, 2). As a scavenger, it searches for other arthropods that were active during the night and early morning but did not retreat quickly enough into their daytime shelters, and consequently succumbed to the heat and desiccation stress caused by the rising sun. In contrast to *C. bombycina*, other species of desert ants stop foraging and retreat to their underground burrows at surface temperatures of 35–45 °C (refs 3–8). The silver ants, however, start their foraging activity only then and continue to forage until their body temperature reaches the critical thermal maximum of 53.6 ± 0.8 °C (for definition and methods, see legend to Fig. 1*a*). This is the highest critical thermal maximum value recorded so far for any terrestrial animal[9,10].

Furthermore, although other *Cataglyphis* species inhabiting more mesic habitats, for example *C. bicolor*, are active during the entire course of the day (Fig. 1*a*)[11], *C. bombycina* confines its foraging activity to an extremely narrow time range. During this period, a colony's forager force, consisting of a few hundred individuals, leaves its nest in a dramatic 'outburst' lasting for only a few minutes ($t_{\frac{1}{2}} = 3.6 \pm 0.6$ min; Fig. 1*b*). This outburst occurs when the temperature measured at ant height (4 mm above the surface) has risen to 46.5 ± 2.1 °C (Table 1). Owing to the ant's small body size (9.72 ± 2.63 mg) and resultant low thermal inertia, its body temperature will be very close to the temperature measured at ant height[12,13]. (Vertical temperature gradients above ground were measured at 15-min intervals using an array of copper-constantan thermocouples mounted at 0, 2, 4, 6, 10, 20, 100 and 200 mm above the sand surface and connected to a data logger.)

As a result, the foraging activity of *C. bombycina* is compressed into a small thermal window, with a maximum width of 7 °C (46.5–53.6 °C; Fig. 2*A*). This thermal window is so close to the ant's upper lethal temperature that the animals must spend at least 30 per cent, and sometimes up to 75 per cent, of their foraging time in thermal refuges (Fig. 2*A*) by pausing on the tops of stalks of dry vegetation where they encounter much

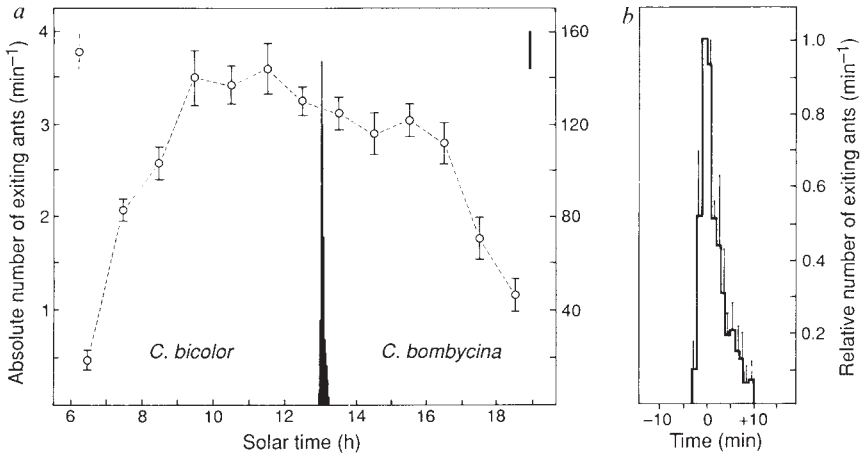

FIG. 1 *a*, Diel foraging activity patterns of *Cataglyphis bicolor* (left ordinate) and *C. bombycina* (right ordinate) recorded in the shrub desert of the North African sahel and the Saharan sand-dune desert, respectively. Foraging activity is expressed as numbers of ants leaving the nest per minute. In *C. bicolor*, means ± s.d. are given for 12 nests. In *C. bombycina*, the figure depicts the foraging 'outburst' of one individual nest. *b*, Time course of the foraging outburst of *C. bombycina* as computed from the data of four outbursts recorded on four consecutive days at one nest (mean + s.d.).